THE JOURNAL OF PHYSICAL CHEMISTRY LETTERS
A JOURNAL OF THE AMERICAN CHEMICAL SOCIETY

pubs.acs.org/JPCL

Letter

Unveiling Argon's Hidden Reactivity: Discovery of Argon Hydroxide Cations at the Air–Water Interface of Microdroplets

Abhijit Nandy, Anitesh Rana, Pragya Pahchan, Deepsikha Kalita, Debasish Koner, and Shibdas Banerjee*

Cite This: *J. Phys. Chem. Lett.* 2026, 17, 389–396

Read Online

ACCESS | Metrics & More | Article Recommendations | Supporting Information

ABSTRACT: Argon is the third most abundant gas in the atmosphere and is regarded as chemically inert. Unlike many other atmospheric gases that have undergone fixation over geological time scales, argon has not been known to form stable compounds. Contrary to this century-old belief, we report that argon can react at the surface of tiny water droplets suspended in air to form argon hydroxide cations ($[ArOH]^+$) at room temperature. Remarkably, this species can be generated and maintained in equilibrium within an aerosol vial for extended periods, following real-time monitoring by mass spectrometry. Mechanistic analysis suggests that the water microdroplet surface carries a net charge and, during its evolution in air into smaller droplets, generates corona discharge, producing $[ArOH]^+$ at the air–water interface. Given the ubiquitous presence of water microdroplets in nature, this reaction of argon with water redefines the landscape of noble gas chemistry on Earth and beyond.

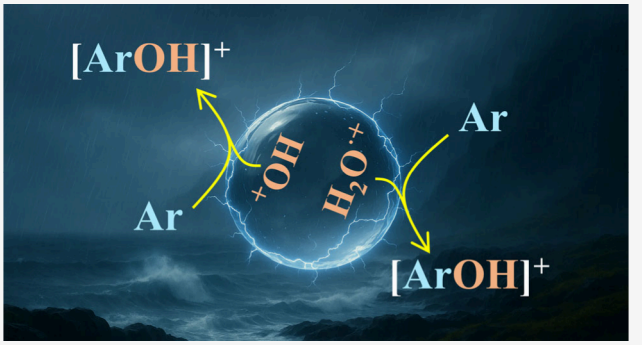

In the Earth's atmosphere, argon has long been known to be a chemically inert gas since its discovery in 1894 by Lord Rayleigh and Sir William Ramsay.[1] This exceptional chemical stability is attributed to its closed-shell electronic configurations. Although it is the third most abundant atmospheric gas, comprising 0.93% by volume, argon has remained a largely passive component, showing strong resistance to fixation or chemical transformation, unlike many other atmospheric gases. Although argon fluorohydride (HArF) has been synthesized under extreme laboratory conditions using a cryogenic matrix at 7.5 K, it remains the only known synthetic argon compound to date.[2] Likewise, the recent detection of argon hydride cation (ArH^+) in the Crab Nebula marked the first and only confirmed noble gas molecule in space, formed under conditions of high ionizing radiation and low-density plasma.[3] Though the possibility of finding a few other argon compounds is further warranted under astrophysical conditions[4] and demonstrated under high-energy plasma or discharge environments,[5−7] finding the ambient argon compound is seemingly forbidden as it would violate long-established chemical principles rooted in atomic structure, thermodynamics, and empirical experience.

Water microdroplets are omnipresent across Earth's natural systems (cloud, rain, fog, sea spray, etc.) and play critical roles in climate, supporting our lives. Recent studies indicated that chemical reactions behave in fundamentally different ways at the air–water interface of microdroplets compared to bulk water.[8−25] In our recent investigations, we detected feeble corona discharge arising at the surface of airborne water microdroplets,[23] a phenomenon later referred to as "microlightning" by Zare and co-workers following the detection of light emission from such droplets.[26,27] We further demonstrated that this interfacial electrical discharge can facilitate nitrogen fixation under ambient conditions, enabling the activation of otherwise inert molecular bonds using only water without the need for catalysts.[23] This finding inspired us to explore whether the discharge-like environment at the surface of water microdroplets could similarly trigger the chemical reactivity of argon. Indeed, we report here that argon reacts at the surface of water microdroplets, generating argon hydroxide cation $[ArOH]^+$, the first-ever ambient argon compound found on Earth. This finding is like watching a long-silent element breaks the rules of its own identity, changing how we understand the chemical reactivity of this inert gas.

Observation of the Phenomenon. When pure water was aerosolized or evaporated in the open air using different methods (steaming, spraying, bubbling, etc.), simulating the formation of airborne microdroplets in front of a high-resolution mass spectrometer, a mysterious ion signal at m/z

Received: October 30, 2025
Revised: December 17, 2025
Accepted: December 18, 2025
Published: December 26, 2025

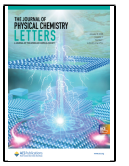

https://doi.org/10.1021/acs.jpclett.5c03405
J. Phys. Chem. Lett. 2026, 17, 389–396

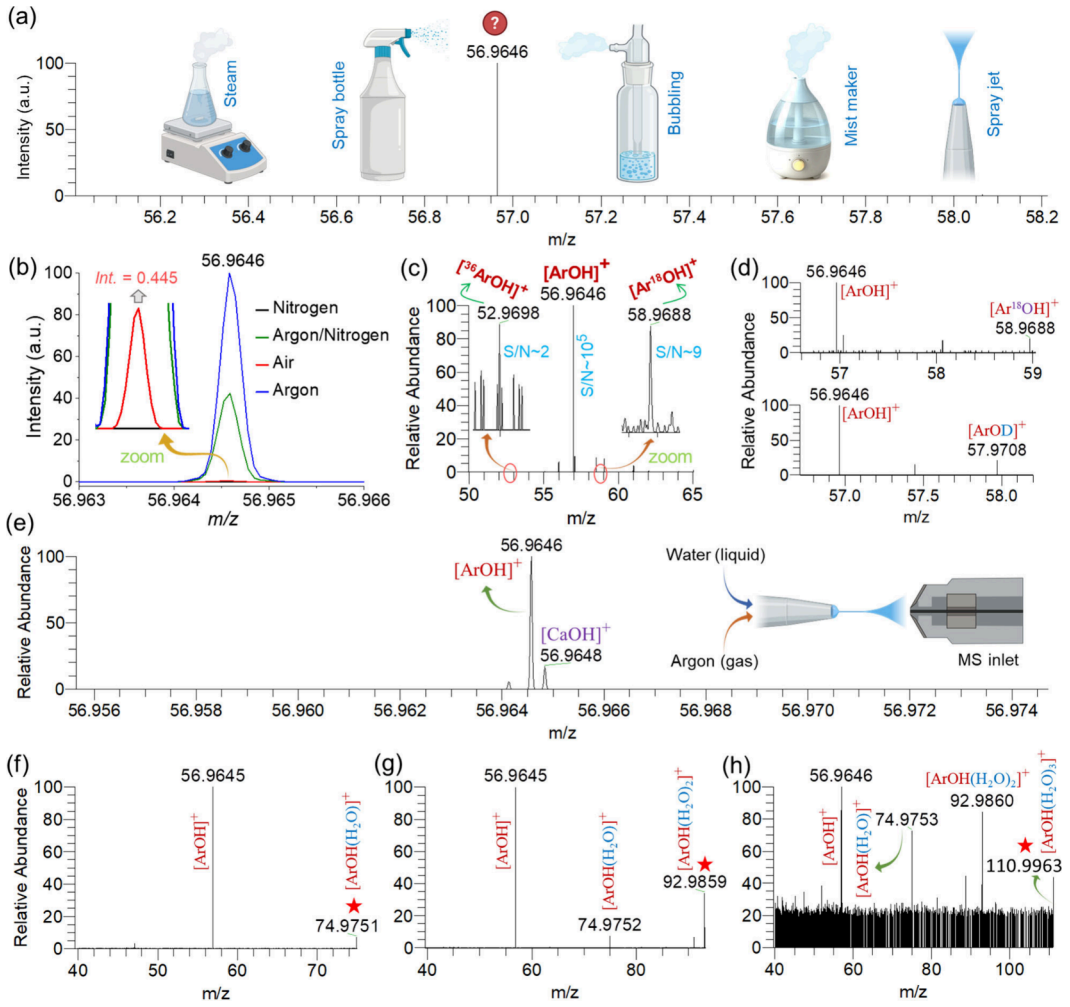

Figure 1. Formation of argon hydroxide cation in the open air. (a) High-resolution mass spectrometric detection of a positively charged species at m/z 56.9646 from aerosolized or evaporating water originating from various sources (insets). (b) Evaluating the formation of this ion upon nebulizing water with nitrogen, nitrogen/argon (1:1, v/v), air, and argon using a 0 V spray source. (c) The exact mass (0 ppm error) and isotopic pattern confirm the identity of the ion as the argon hydroxide cation. (d) Detection of isotopically labeled argon hydroxide cation upon spraying ^{18}O-enriched water (top panel) and deuterium-enriched water (bottom panel). (e) Ultrahigh resolution (R = 500000) mass spectrometric confirmation of $[ArOH]^+$ species obtained from nebulizing water with argon at 0 V (inset). (f–h) Tandem mass spectrometric characterization of the argon hydroxide cation noncovalently bound to one (e), two (f), and three (g) water molecules (asterisked), showing the sequential loss of water during fragmentation.

56.9646 was detected consistently (Figure 1a) across all experiments (Figure S1a–e). To further characterize this species, we employed a 0 V spray source setup as described in the Materials and Methods section. Nebulization of water with nitrogen, air, and argon revealed a distinct dependence of the above ion signal on the carrier gas: the peak was absent with nitrogen (black trace), weakly present with air, and markedly intense with argon (Figure 1b), implicating argon as a constituent element of the observed ion. The weak signal observed for this species when air was used as the carrier gas can be attributed to the low abundance (<1%) of argon in air. This observation remained consistent when the spray source was operated inside both argon- and nitrogen-filled glove boxes, with the aerosol subsequently transferred to the mass spectrometer through a stainless-steel capillary, effectively isolating the spray from exposure to laboratory air (Figure S2). Since the ion (m/z 56.9646) was not detected in the carrier gas alone (Figure S3), the interaction between water microdroplets and argon appears essential for forming this species. The critical role of water in the formation of the observed ion is further supported by its detection upon aerosolization of an aqueous solvent, whereas no corresponding signal was observed when organic solvents were aerosolized under the same conditions (Figure S4).

Characterization of the Species. The high mass accuracy (0 ppm error) analysis suggests the species to be the argon hydroxide cation, $[ArOH]^+$ (Figure 1c). This is further corroborated by the detection of associated isotopic peaks corresponding to the natural abundances of ^{36}Ar and ^{18}O, albeit at trace intensity levels (insets of Figure 1c). Moreover, when ^{18}O-enriched (2:1, v/v) or deuterium-enriched (5:1, v/v) water was nebulized using argon, the corresponding heavier isotopologues of the argon hydroxide cation were detected (Figure 1d), albeit at lower abundances, likely due to the preferential surface affinity of the lighter water isotopologues, as demonstrated in our earlier study.[28] These results further suggest that the water surface, i.e., the liquid–gas interface, is the probable reaction zone for the formation of $[ArOH]^+$ species.

https://doi.org/10.1021/acs.jpclett.5c03405
J. Phys. Chem. Lett. 2026, 17, 389–396

It is essential to clarify that the assignment of the ion is not solely based on the empirical observations (Figure 1a–d and Figures S1–S4) but also on the fact that no alternative elemental composition fits the m/z 56.9646 value within the constraints of high mass accuracy (<1 ppm), thereby justifying the results in Figure 1b. Upon further resolution using an ultrahigh-resolution mass spectrometer (Thermo Orbitrap Fusion MS), the $[ArOH]^+$ ion signal was clearly distinguished from a weak isobaric interference, likely corresponding to $[CaOH]^+$ (Figure 1e). Similarly, another hybrid ion trap–orbitrap mass spectrometer successfully detected $[ArOH]^+$ upon nebulizing water with argon, but not with nitrogen (Figure S5). These consistent and reproducible observations across multiple high-resolution instruments located at different sites further validate the robustness of the findings.

Evaluation of the mass spectral data (Figure S6) also revealed that $[ArOH]^+$ can exist in hydrated forms by adducting with up to three water molecules, which were further characterized through tandem mass spectrometric (MS/MS) study (Figure 1f–h). The energy-resolved MS/MS analysis (Figure S7) further confirmed the weak association of H_2O molecules with the $[ArOH]^+$ species, likely mediated through hydrogen bonding.

We also observed that the nature and source of water significantly influence the generation of $[ArOH]^+$, with variations in water quality parameters such as pH, conductivity, and total dissolved solids (TDS) playing a critical role (Figure S8). Microdroplets generated from pure deionized water exhibited the highest $[ArOH]^+$ signal, whereas those derived from contaminated sources such as tap water or rainwater showed reduced production of $[ArOH]^+$. Notably, while nebulization of seawater (characterized by high TDS) did not yield detectable $[ArOH]^+$ (data not shown), the ion was observed upon evaporating seawater under laboratory conditions (Figure S9). Thus, the results obtained from atmospheric water samples (such as sprayed rainwater and seawater vapor, Figure S8) support the formation of $[ArOH]^+$ through the reaction of argon gas with water microdroplets under open-air conditions.

While accurate quantification of the $[ArOH]^+$ species would ideally require a dedicated standard, which is infeasible here, we attempted for an estimation of its abundance using a highly water-soluble, unipositive ion such as Cs^+ as a reference. Since both $[ArOH]^+$ and Cs^+ are intrinsically charged, we assumed their mass spectrometric detection efficiencies to be approximately comparable. Based on this assumption, we generated a calibration plot for the Cs^+ ion, which provided a rough guideline for estimating the concentration of $[ArOH]^+$ across various aerosol/mist sources (Figure S10). Using this approach, we found that the concentration of $[ArOH]^+$ in microdroplets ranges from parts per trillion (ppt) to parts per billion (ppb), depending on the mode of water aerosolization. For instance, $[ArOH]^+$ exhibited the lowest abundance in the seawater vapor, with an estimated concentration of ~ 4 ppt, whereas its highest abundance, with approximately 5 ppb, was observed in microdroplets generated by argon-driven nebulization using a 0 V spray jet. Likewise, the mist generated by a household humidifier produced $[ArOH]^+$ at an estimated concentration of approximately 0.7 ppb in microdroplets (Figure S10).

Assessment of the Stability of the Species. We designed a custom glass reaction chamber to aerosolize water using an ultrasonic fogger, with the resulting microdroplets confined within the argon-purged chamber (Figure 2a). The aerosol was subsequently transferred through a borosilicate

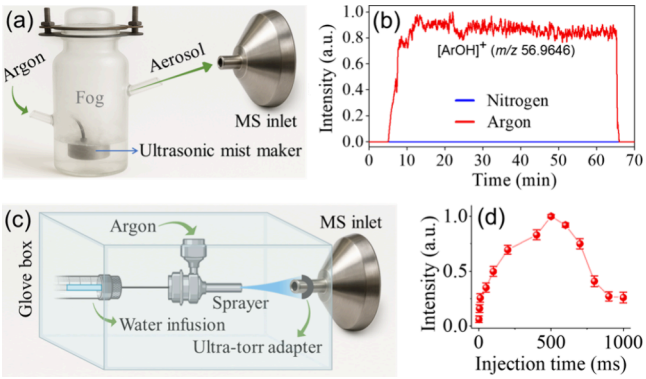

Figure 2. Formation and stability of the argon hydroxide cation. (a) Experimental setup for continuous real-time monitoring of $[ArOH]^+$ in laboratory-generated fog within an argon-purged reaction chamber. (b) Temporal profile of $[ArOH]^+$ ion abundance (red trace) recorded over a 1-h period, with fog maker (shown in A) operation initiated at 5 min and stopped at 65 min. In the control experiment using nitrogen as the purging gas, $[ArOH]^+$ was not detected (blue trace). (c) Illustration of a 0 V spray setup inside a glovebox, enabling MS analysis of internal aerosols while preventing external contamination. (d) A plot of $[ArOH]^+$ ion intensity as a function of maximum ion injection time, highlighting its accumulation behavior and stability in the gas phase.

capillary into the mass spectrometer for analysis (Figure S11) in real time. The $[ArOH]^+$ species was detected almost immediately after the fogger was activated, with its signal intensity gradually rising to a maximum within a few minutes and remaining at this level for an extended duration, until the fogger was turned off (Figure 2b). This result clearly demonstrates that the species was generated in the aerosol chamber, establishing a chemical equilibrium, evidenced by the steady concentration of the $[ArOH]^+$ over time in the reaction between water and argon in the container. That the presence of the species was directly correlated with the existence of the aerosol or water vapor was further supported by experiments in which water microdroplets or vapor (from various sources) were exposed to air or argon, resulting in continuous detection of $[ArOH]^+$ throughout the exposure period (Figure S12). Collectively, these results also indicate that $[ArOH]^+$ possesses sufficient stability to enable mass spectrometric sampling on a time scale of seconds and detection on a time scale of milliseconds.[29,30] The species could also be stored in the gas phase (within the C-trap of Thermo Exploris 120 MS) for approximately half a second, as evidenced by a plot of its ion signal intensity versus maximum ion injection time, showing peak ion counts at 500 ms (Figure 2c–d).

Mechanistic Investigation. A custom-designed spray source was interfaced with the mass spectrometer (Figure 3a) to investigate the mechanistic aspects of $[ArOH]^+$ formation. As previously discussed, the water surface is known to facilitate unusual chemical reactivity due to its distinct physical and chemical properties.[8−25,31−41] In the present study, we also demonstrate that the reaction between argon and water most likely occurs at the gas–liquid interface of microdroplets, where the reaction exhibits a surface-sensitive behavior, reflecting a dependence on droplet surface area and charge. For example, tuning the spray parameters, such as

https://doi.org/10.1021/acs.jpclett.5c03405
J. Phys. Chem. Lett. 2026, 17, 389−396

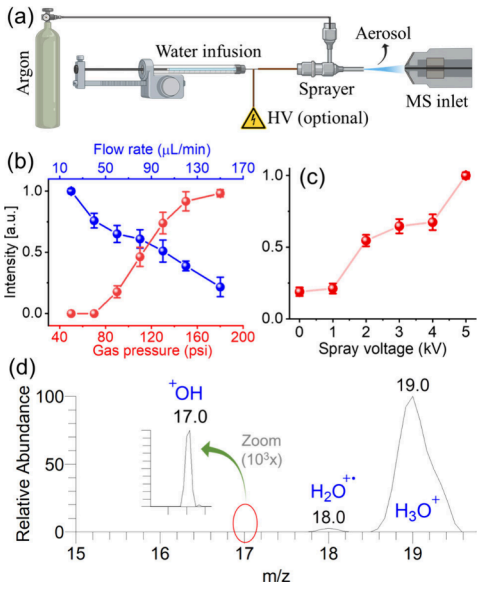

Figure 3. Experimental investigation of the reaction mechanism. (a) Diagram of an ESI-MS experimental setup used to monitor the impact of spray parameters on $[ArOH]^+$ ion abundance. Plot of $[ArOH]^+$ ion signal intensity as a function of various spray parameters: (b) nebulizing gas (argon) pressure and water flow rate, and (c) spray potential. All intensity data points were collected relative to the ion signal of protonated dimethylformamide, which was added to the water at a concentration of 0.01 ppm. (d) ESI-MS data from an ion trap mass spectrometer in the low mass range, obtained by spraying deionized water under a + 5 kV potential using argon as the nebulizing gas.

reducing the solvent flow rate, increasing the nebulizing gas pressure led to smaller microdroplets with higher surface-to-volume ratios,[17,30,42,43] thereby enhancing the reaction efficiency (Figure 3b).

Moreover, the application of a positive spray potential, which promotes the formation of overall positively charged microdroplet surfaces,[29,30,32] resulted in a significant improvement in the reaction efficiency (Figure 3c). Molecular dynamics simulations further suggested that when an aqueous solution containing argon atoms forms microdroplets, argon rapidly migrates to the surface of the droplet and finally evaporates from the aqueous droplet within half nanosecond (see Figure S13). This finding aligns with the above experimental results and supports the notion that the gas–liquid interface of microdroplets serves as the reaction zone for argon.

The micron sized droplets are almost never found neutral, whether formed naturally (Lenard effect) or produced in the laboratory; they always carry net charge arising from an excess of H_3O^+ or OH^-.[23,26,44−46] When a fluid jet breaks into droplets (Rayleigh–Plateau instability), the breakup is not symmetric. Even a tiny imbalance in charge distribution (e.g., H^+ and OH^-) get frozen into droplets, producing some positively charged droplets and some negatively charged droplets. Such charge separation is further amplified when water is aerosolized under high-pressure nebulization, as recently demonstrated by Zare and co-workers.[26] Central to this behavior is the electrical double layer at the air–water interface, characterized by OH^- enrichment at the outermost surface and a subsurface layer rich with counterions (e.g., H^+) immediately beneath it. The OH^- ions stabilize more readily at water-deficient interface (higher hydration enthalpy penalty for H^+) as hydration enthalpies of OH^- and H^+ are −520 kJ mol^{-1} and −1150 kJ mol^{-1}, respectively.[47] Because this interfacial layer carries a net negative charge, and aerodynamic breakup transfers more of this surface layer to the smaller offspring droplet, rendering it overall negatively charged while leaving the larger parent droplets correspondingly positive.[26] During this secondary breakup, a transient localized electric field might be established between the larger positively charged droplet and the smaller negatively charged one, with an estimated magnitude of ~10^9 V/m.[26] As this electric field is much higher than the dielectric strength of air (~3×10^6 V/m), it allows a spark or arc to form by breaking down the surrounding air, ionizing different air molecules.[23,26,27] In other words, this intense localized electric field may trigger plasma chemistry at the air–water interface. This rationale aligns with our detection of Ar^+ in the low-mass region by high-resolution mass spectrometry, a species that may form transiently at the interface (Figure S14), especially when water was nebulized using argon, in agreement with our previous observation.[23]

Alternatively, Colussi demonstrated that excess surface charge on aerosolized water microdroplets generates an electric field that scales directly with the net charge and inversely with droplet radius.[48] Using typical charge values and radii reported for such droplets, he estimated fields on the order of 10^5–10^6 V/m, which may increase further under continuous solvent evaporation and enhancement of surface curvature. Given that the electric field generated by charged aerosolized microdroplets can approach the air-breakdown threshold, interfacial electrical discharge from such droplets may still be expected as a plausible alternative source. Moreover, such a high field can accelerate an electron at the interface or naturally occurring gas-phase electrons produced by cosmic ionizing radiation, enabling them to strip electrons from nearby molecules and initiate an avalanche process that rapidly amplifies the concentrations of electrons and corresponding positive ions.[49] This can also interpret the formation of Ar^+ upon spraying water in the air (Figure S14). A compelling indication that the interfacial plasma chemistry may arise from the threshold electric fields radiated by charged microdroplets is the observation that positively charged water microdroplets also ionize surrounding gas molecules.[50] Indeed, our earlier observation of air breakdown at the surface of sprayed water microdroplets, akin to a microscopic lightning event, provided direct evidence for a strong interfacial electric field capable of initiating energetic reactions, including nitrogen oxide formation and gas-phase ionization.[23] Subsequent literature reports have further validated this finding.[26,27]

Considering the two models discussed above as potential origins of interfacial electrical discharge in microdroplets, we outline below the plausible mechanistic pathways leading to the formation of $[ArOH]^+$. A positive control experiment involving nebulized water sprayed near a corona discharge zone yielded a pronounced increase in the $[ArOH]^+$ signal, accompanied by a weak Ar^+ ion signal (Figure S15), supporting the involvement of electrical discharge in their formation. Spraying water into air yields reactive oxygen species H_2O_2, $O_2^{\bullet-}$, $^{\bullet}OH$, $H_2O^{\bullet+}$, etc.), as proposed in numerous studies.[10,51−55] While their spontaneous formation has been questioned,[56] these species are reliably produced under the pneumatic conditions of spraying, in agreement with many microdroplet reactions of organic substrates that depend on in situ generation of $^{\bullet}OH/H_2O_2$ as the sprayed mixture is

https://doi.org/10.1021/acs.jpclett.5c03405
J. Phys. Chem. Lett. 2026, 17, 389−396

collected in a vial.[57−62] Moreover, it is no wonder that the interfacial plasma-like micro environment can also contribute to the formation of such ROS (Supplementary Note 1).[63−66] Experiments with isotopically labeled water ($H_2{}^{18}O$) confirmed that these ROS likely originate through intertwined pathways involving both interfacial water and atmospheric oxygen.[28,55] Nevertheless, given that sprayed water produces both Ar^+ and OH•, we invoke Occam's razor to propose that $[ArOH]^+$ forms through the direct combination of these two reactive species (Figure 4a). However, other plausible pathways are outlined below.

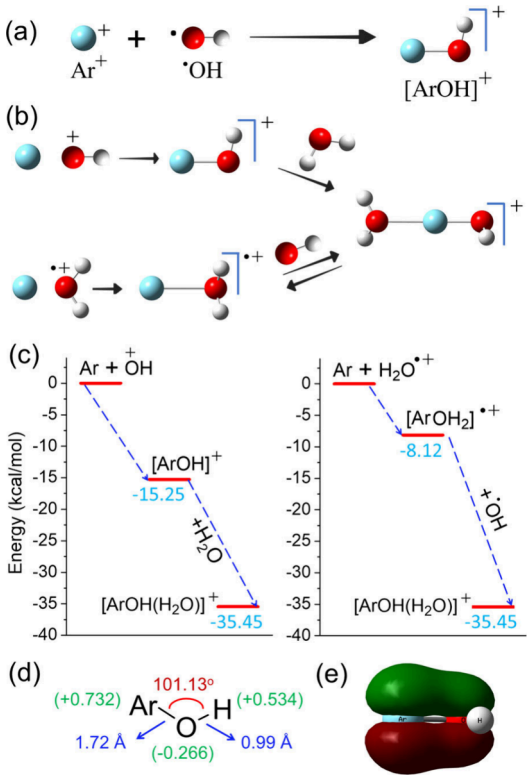

Figure 4. Theoretical insights. (a, b) Schematic diagrams of the three plausible reaction pathways leading to the formation of $[ArOH]^+$, depicted using ball-and-stick models. (c) Potential energy profiles computed at CCSD(T)/aug-cc-pVQZ level of theory for pathways depicted in (b). Only the lowest energy states are shown in the energy profile. Other electronic states are shown in Figure S18. (d) Characteristics of the argon hydroxide cation (singlet) equilibrium configuration computed at CCSD(T)/aug-cc-pV5Z level of theory, showing bond lengths (blue), bond angle (red), and NBO charge distribution on atoms (green). (e) Molecular orbital picture illustrating the bonding interactions in the species obtained from CCSD(T)/aug-cc-pV5Z calculations.

Considering that the surface of water microdroplets creates a corona discharge-like environment, we hypothesized the formation of the hydroxyl cation (OH^+), another ROS that may have previously escaped attention in studies of interfacial microdroplet chemistry due to its fleeting life. When water microdroplets were sprayed at +5 kV using argon as the nebulizing gas in front of an ion trap mass spectrometer, with emphasis on detecting low-mass ions, a weak signal at m/z 17 was observed, potentially corresponding to OH^+, alongside notable signals for $H_2O^{+\cdot}$ (m/z 18) and H_3O^+ (m/z 19) (Figure 3d). Thus, this finding confirms the formation of OH^+ at the air−water interface of microdroplets and also in line with the previous reports on is formation under plasma or discharge environments.[3,67,68]

Given that interfacial corona discharge can generate both OH^+ and $H_2O^{\bullet+}$, we also acknowledge two other mechanistically plausible routes to $[ArOH]^+$ formation, as depicted in Figure 4b−c, based on calculations performed at the CCSD(T)/aug-cc-pVQZ level of theory. In the first pathway, argon reacts exothermically with the highly reactive triplet-state OH^+ to yield $[ArOH]^+$, which may be further stabilized through interaction with one or more water molecules, consistent with experimental observations (Figure 1f−h). The potential source of the OH^+ ion can be assigned to ·OH radical. The formation of ·OH radicals from OH^- ions is thermodynamically favorable on the surface of aqueous microdroplets.[47] Given the feasibility of the formation of high electric field at the air−water interface of microdroplets, as discussed above, the possibility of the formation of OH^+ cations from OH radicals through field-induced polarization has been theoretically examined, as shown in Figure S16. A similar mechanism is proposed for the generation of $H_2O^{\bullet+}$ radical cations, as illustrated in Figure S17. In the presence of a strong electric field, interfacial H_2O can polarize to transfer one electron to the droplet to form a $H_2O^{\bullet+}$ cation. This has also been suggested earlier by Cooks and co-workers.[54] Given the detection of the $H_2O^{\bullet+}$ ion signal (Figure 3d), we also explored a second reaction pathway (Figure 4b,c) involving the interaction of argon with $H_2O^{\bullet+}$, which can exothermically yield the $[Ar(H_2O)]^{\bullet+}$ complex. This cationic argon−water adduct can be further stabilized by reacting with a hydroxyl radical, leading to the formation of $[ArOH(H_2O)]^+$. The breakdown of this species can form $[ArOH]^+$ (Figure 1f) at the interface.

The electronic structure of the most stable singlet state of $[ArOH]^+$ was investigated using high-level CCSD(T)/aug-cc-pV5Z calculations. The optimized geometry reveals an Ar−O bond length of 1.72 Å and an Ar−O−H bond angle of 101.13°. Natural bond orbital (NBO) analysis indicates that the highest positive charge density is localized on the argon atom (Figure 4d). The bonding orbital of $[ArOH]^+$ was analyzed and is illustrated in Figure 4e. The molecular orbital (MO) representation highlights the predominant π-character of the Ar−O bond. This bonding interaction arises from atomic orbitals of argon and oxygen, each contributing over 90% p-character, resulting in a moderately strong π-type bond between the Ar and O atoms. The harmonic vibrational frequencies, computed at the CCSD(T)/aug-cc-pV5Z level of theory, were found to be 640.7 cm^{-1} (Ar−O stretching), 1349.9 cm^{-1} (bending mode), and 3539.2 cm^{-1} (O−H stretching), respectively.

Thus, combined experimental and theoretical investigations suggest that the interfacial electrical discharge facilitates the formation of $[ArOH]^+$ at the water microdroplet surface. It is important to clarify that although the droplet surface microenvironment exhibits characteristics akin to an electrical discharge capable of activating inert argon, the overall conditions under which the droplets are exposed remain ambient, thereby demonstrating that argon activation occurs under ambient conditions (e.g., room temperature and atmospheric pressure).

In summary, over a century after the discovery of argon and its subsequent characterization as chemically inert, the present study introduces a notable exception to noble gas chemistry by demonstrating that argon can undergo an unprecedented

https://doi.org/10.1021/acs.jpclett.5c03405
J. Phys. Chem. Lett. 2026, 17, 389−396

reaction under ambient conditions to form a stable argon hydroxide cation ($[ArOH]^+$) at the surface of water microdroplets. Remarkably, while isolated $[ArOH]^+$ species exhibit stability for about half a second under vacuum conditions, they persist in equilibrium for extended periods within aqueous aerosols. This suggests a uniquely favorable chemical environment at the gas−liquid interface of microdroplets that enhances the species stability. Mechanistic insights from mass spectrometry suggest that the reaction may proceed through multiple pathways within the plasma-like microenvironment at the air−water interface of microdroplets, involving Ar^+, OH^+, and $H_2O^{\bullet+}$ species generated at the interface. Given the ubiquitous presence of aqueous aerosols on Earth and the widespread cosmic abundance of argon, these findings significantly revise our understanding of the reactivity of argon. Furthermore, this discovery opens new avenues for exploring analogous aqueous reactions in extraterrestrial environments and raises the intriguing prospect of employing $[ArOH]^+$ as a chemical marker for identifying exotic aqueous processes occurring elsewhere in the cosmos.

■ ASSOCIATED CONTENT

Supporting Information

The Supporting Information is available free of charge at https://pubs.acs.org/doi/10.1021/acs.jpclett.5c03405.

Materials and methods, mass spectral data (PDF)

Transparent Peer Review report available (PDF)

■ AUTHOR INFORMATION

Corresponding Author

Shibdas Banerjee − *Department of Chemistry, Indian Institute of Science Education and Research Tirupati, Tirupati 517619, India;* orcid.org/0000-0002-3424-8157; Email: shibdas@iisertirupati.ac.in

Authors

Abhijit Nandy − *Department of Chemistry, Indian Institute of Science Education and Research Tirupati, Tirupati 517619, India*

Anitesh Rana − *Department of Chemistry, Indian Institute of Science Education and Research Tirupati, Tirupati 517619, India*

Pragya Pahchan − *Department of Chemistry, Indian Institute of Science Education and Research Tirupati, Tirupati 517619, India*

Deepsikha Kalita − *Department of Chemistry, Indian Institute of Technology Hyderabad, Kandi 502284, India*

Debasish Koner − *Department of Chemistry, Indian Institute of Technology Hyderabad, Kandi 502284, India;* orcid.org/0000-0002-5116-4908

Complete contact information is available at: https://pubs.acs.org/10.1021/acs.jpclett.5c03405

Notes

The authors declare no competing financial interest.

■ ACKNOWLEDGMENTS

S.B. gratefully acknowledges financial support from the Science and Engineering Research Board (SERB), Government of India (Grant No. CRG/2022/002676). D.K. acknowledges support from the Department of Science and Technology (DST), India, through the INSPIRE faculty fellowship (Grant No. DST/INSPIRE/04/2019/002108). A.N. acknowledges the award of a Prime Minister's Research Fellowship (PMRF), Government of India. The authors gratefully acknowledge D. Venkataramana (Thermo Fisher Scientific, India) for his valuable assistance during the ultrahigh-resolution MS experiments.

■ REFERENCES

(1) Strutt, R. J.; Ramsay, W. I. Argon, a new constituent of the atmosphere. *Proc. R. Soc. London* **1895**, *57* (340-346), 265−287.

(2) Khriachtchev, L.; Pettersson, M.; Runeberg, N.; Lundell, J.; Räsänen, M. A stable argon compound. *Nature* **2000**, *406* (6798), 874−876.

(3) Barlow, M. J.; Swinyard, B. M.; Owen, P. J.; Cernicharo, J.; Gomez, H. L.; Ivison, R. J.; Krause, O.; Lim, T. L.; Matsuura, M.; Miller, S.; Olofsson, G.; Polehampton, E. T. Detection of a Noble Gas Molecular Ion, 36ArH+, in the Crab Nebula. *Science* **2013**, *342* (6164), 1343−1345.

(4) Theis, R. A.; Fortenberry, R. C. Potential interstellar noble gas molecules: ArOH+ and NeOH+ rovibrational analysis from quantum chemical quartic force fields. *Mol. Astrophys.* **2016**, *2*, 18−24.

(5) Arnold, T.; Harvey, J. N.; Weiss, D. J. An experimental and theoretical investigation into the use of H2 for the simultaneous removal of ArO+ and ArOH+ isobaric interferences during Fe isotope ratio analysis with collision cell based Multi-Collector Inductively Coupled Plasma Mass Spectrometry. *Spectrochim. Acta Part B: Atom. Spectro.* **2008**, *63* (6), 666−672.

(6) Wagner, J. P.; McDonald, D. C., II; Duncan, M. A. An Argon-Oxygen Covalent Bond in the ArOH+ Molecular Ion. *Angew. Chem., Int. Ed.* **2018**, *57* (18), 5081−5085.

(7) Koskinen, J. T.; Cooks, R. G. Novel Rare Gas Ions BXe+, BKr+, and BAr+ Formed in a Halogen/Rare Gas Exchange Reaction. *J. Phys. Chem. A* **1999**, *103* (48), 9565−9568.

(8) Lee, J. K.; Banerjee, S.; Nam, H. G.; Zare, R. N. Acceleration of reaction in charged microdroplets. *Q. Rev. Biophys.* **2015**, *48* (4), 437−444.

(9) Banerjee, S.; Gnanamani, E.; Yan, X.; Zare, R. N. Can all bulk-phase reactions be accelerated in microdroplets? *Analyst* **2017**, *142* (9), 1399−1402.

(10) Lee, J. K.; Walker, K. L.; Han, H. S.; Kang, J.; Prinz, F. B.; Waymouth, R. M.; Nam, H. G.; Zare, R. N. Spontaneous generation of hydrogen peroxide from aqueous microdroplets. *Proc. Natl. Acad. Sci. U. S. A.* **2019**, *116* (39), 19294−19298.

(11) Wei, Z.; Li, Y.; Cooks, R. G.; Yan, X. Accelerated Reaction Kinetics in Microdroplets: Overview and Recent Developments. *Annu. Rev. Phys. Chem.***2020**, *71* (71), 31−51.

(12) Gnanamani, E.; Yan, X.; Zare, R. N. Chemoselective N-Alkylation of Indoles in Aqueous Microdroplets. *Angew. Chem., Int. Ed.* **2020**, *59* (8), 3069−3072.

(13) Nandy, A.; Kumar, A.; Mondal, S.; Koner, D.; Banerjee, S. Spontaneous Generation of Aryl Carbocations from Phenols in Aqueous Microdroplets: Aromatic SN1 Reactions at the Air-Water Interface. *J. Am. Chem. Soc.* **2023**, *145* (29), 15674−15679.

(14) Nandy, A.; T, H.; Kalita, D.; Koner, D.; Banerjee, S. Stabilizing Highly Reactive Aryl Carbanions in Water Microdroplets: Electrophilic Ipso-Substitution at the Air-Water Interface. *JACS Au* **2024**, *4* (11), 4488−4495.

(15) Nandy, A.; Rana, A.; Shibata, N.; Banerjee, S. Breaking the Strongest Organic Bonds by Water: Defluorosubstitutions at the Air-Water Interface of Microdroplets. *J. Am. Chem. Soc.* **2025**, *147*, 22542.

(16) Nandy, A.; Murmu, G.; Rana, A.; Saha, S.; Banerjee, S. Sprayed Microdroplets Architect a Polyoxometalate Framework. *Angew. Chem., Int. Ed.* **2025**, *64* (24), No. e202424745.

(17) Gong, K.; Nandy, A.; Song, Z.; Li, Q.-S.; Hassanali, A.; Cassone, G.; Banerjee, S.; Xie, J. Revisiting the Enhanced Chemical Reactivity in Water Microdroplets: The Case of a Diels-Alder Reaction. *J. Am. Chem. Soc.* **2024**, *146* (46), 31585−31596.

(18) Mohajer, M. A.; Basuri, P.; Evdokimov, A.; David, G.; Zindel, D.; Miliordos, E.; Signorell, R. Spontaneous formation of urea from carbon dioxide and ammonia in aqueous droplets. *Science* **2025**, *388* (6754), 1426−1430.
(19) Spoorthi, B. K.; Debnath, K.; Basuri, P.; Nagar, A.; Waghmare, U. V.; Pradeep, T. Spontaneous weathering of natural minerals in charged water microdroplets forms nanomaterials. *Science* **2024**, *384* (6699), 1012−1017.
(20) Song, X.; Basheer, C.; Zare, R. N. Water Microdroplets-Initiated Methane Oxidation. *J. Am. Chem. Soc.* **2023**, *145* (50), 27198−27204.
(21) Chen, H.; Wang, R.; Chiba, T.; Foreman, K.; Bowen, K.; Zhang, X. Designer "Quasi-Benzyne": The Spontaneous Reduction of Ortho-Diiodotetrafluorobenzene on Water Microdroplets. *J. Am. Chem. Soc.* **2024**, *146* (15), 10979−10983.
(22) Zhu, C.; Pham, L. N.; Yuan, X.; Ouyang, H.; Coote, M. L.; Zhang, X. High Electric Fields on Water Microdroplets Catalyze Spontaneous and Fast Reactions in Halogen-Bond Complexes. *J. Am. Chem. Soc.* **2023**, *145* (39), 21207−21212.
(23) Kumar, A.; Avadhani, V. S.; Nandy, A.; Mondal, S.; Pathak, B.; Pavuluri, V. K. N.; Avulapati, M. M.; Banerjee, S. Water Microdroplets in Air: A Hitherto Unnoticed Natural Source of Nitrogen Oxides. *Anal. Chem.* **2024**, *96* (26), 10515−10523.
(24) Song, X.; Basheer, C.; Xia, Y.; Li, J.; Abdulazeez, I.; Al-Saadi, A. A.; Mofidfar, M.; Suliman, M. A.; Zare, R. N. One-step Formation of Urea from Carbon Dioxide and Nitrogen Using Water Microdroplets. *J. Am. Chem. Soc.* **2023**, *145* (47), 25910−25916.
(25) Banerjee, S.; Prakash, H.; Mazumdar, S., Evidence of Molecular Fragmentation inside the Charged Droplets Produced by Electrospray Process. *J. Am. Soc. Mass Spectrom.* **2011**, *22* (10). DOI: 10.1007/s13361-011-0188-7
(26) Xia, Y.; Xu, J.; Li, J.; Chen, B.; Dai, Y.; Zare, R. N. Visualization of the Charging of Water Droplets Sprayed into Air. *J. Phys. Chem. A* **2024**, *128* (28), 5684−5690.
(27) Meng, Y.; Xia, Y.; Xu, J.; Zare, R. N. Spraying of water microdroplets forms luminescence and causes chemical reactions in surrounding gas. *Sci. Adv.* **2025**, *11* (11), No. eadt8979.
(28) Nandy, A.; Mondal, S.; Koner, D.; Banerjee, S. Heavy Water Microdroplet Surface Enriches the Lighter Isotopologue Impurities. *J. Am. Chem. Soc.* **2024**, *146* (28), 19050−19058.
(29) Kebarle, P.; Tang, L. From ions in solution to ions in the gas phase - the mechanism of electrospray mass spectrometry. *Anal. Chem.* **1993**, *65* (22), 972A−986A.
(30) Banerjee, S.; Mazumdar, S. Electrospray Ionization Mass Spectrometry: A Technique to Access the Information beyond the Molecular Weight of the Analyte. *Int. J. Anal. Chem.* **2012**, *2012* (1), 282574.
(31) Banerjee, S.; Zare, R. N. Syntheses of Isoquinoline and Substituted Quinolines in Charged Microdroplets. *Angew. Chem., Int. Ed.* **2015**, *54* (49), 14795−9.
(32) Banerjee, S. On the stability of carbocation in water microdroplets. *Int. J. Mass Spectrom.* **2023**, *486*, 117024.
(33) Colussi, A. J.; Enami, S.; Ishizuka, S. Hydronium Ion Acidity Above and Below the Interface of Aqueous Microdroplets. *ACS Earth Space Chem.* **2021**, *5* (9), 2341−2346.
(34) Li, K.; Gong, K.; Liu, J.; Ohnoutek, L.; Ao, J.; Liu, Y.; Chen, X.; Xu, G.; Ruan, X.; Cheng, H.; Han, J.; Sui, G.; Ji, M.; Valev, V. K.; Zhang, L. Significantly accelerated photochemical and photocatalytic reactions in microdroplets. *Cell Rep. Phys. Sci.* **2022**, *3* (6), 100917.
(35) Brown, E. K.; Rovelli, G.; Wilson, K. R. pH jump kinetics in colliding microdroplets: accelerated synthesis of azamonardine from dopamine and resorcinol. *Chem. Sci.* **2023**, *14* (23), 6430−6442.
(36) Xiong, H.; Lee, J. K.; Zare, R. N.; Min, W. Strong Concentration Enhancement of Molecules at the Interface of Aqueous Microdroplets. *J. Phys. Chem. B* **2020**, *124* (44), 9938−9944.
(37) Xiong, H.; Lee, J. K.; Zare, R. N.; Min, W. Strong Electric Field Observed at the Interface of Aqueous Microdroplets. *J. Phys. Chem. Lett.* **2020**, *11* (17), 7423−7428.
(38) Hao, H.; Leven, I.; Head-Gordon, T. Can electric fields drive chemistry for an aqueous microdroplet? *Nat. Commun.* **2022**, *13* (1), 280.
(39) Heindel, J. P.; LaCour, R. A.; Head-Gordon, T. The role of charge in microdroplet redox chemistry. *Nat. Commun.* **2024**, *15* (1), 3670.
(40) Chen, C. J.; Williams, E. R. The role of analyte concentration in accelerated reaction rates in evaporating droplets. *Chem. Sci.* **2023**, *14* (18), 4704−4713.
(41) Enami, S.; Stewart, L. A.; Hoffmann, M. R.; Colussi, A. J. Superacid Chemistry on Mildly Acidic Water. *J. Phys. Chem. Lett.* **2010**, *1* (24), 3488−3493.
(42) Gao, D.; Jin, F.; Lee, J. K.; Zare, R. N. Aqueous microdroplets containing only ketones or aldehydes undergo Dakin and Baeyer-Villiger reactions. *Chem. Sci.* **2019**, *10* (48), 10974−10978.
(43) Xia, Z.; Williams, E. R. Effect of droplet lifetime on where ions are formed in electrospray ionization. *Analyst* **2019**, *144* (1), 237−248.
(44) Lenard, P. Ueber die Electricität der Wasserfälle. *Annalen der Physik* **1892**, *282* (8), 584−636.
(45) Zhang, C.; Wu, Z.; Wang, C.; Li, H.; Li, Z.; Lin, J.-M. Hydrated negative air ions generated by air-water collision with TiO2 photocatalytic materials. *RSC Adv.* **2020**, *10* (71), 43420−43424.
(46) Zilch, L. W.; Maze, J. T.; Smith, J. W.; Ewing, G. E.; Jarrold, M. F. Charge Separation in the Aerodynamic Breakup of Micrometer-Sized Water Droplets. *J. Phys. Chem. A* **2008**, *112* (51), 13352−13363.
(47) Colussi, A. J. Mechanism of Hydrogen Peroxide Formation on Sprayed Water Microdroplets. *J. Am. Chem. Soc.* **2023**, *145* (30), 16315−16317.
(48) Colussi, A. J. Physical Chemistry of Water Microdroplets. *J. Phys. Chem. Lett.* **2025**, *16* (13), 3366−3370.
(49) Chen, C. J.; Avadhani, V. S.; Williams, E. R. Electronic Excitation and High-Energy Reactions Originate From Anionic Microdroplets Formed by Electrospray or Pneumatic Nebulization. *Angew. Chem., Int. Ed.* **2025**, *64* (19), No. e202424662.
(50) He, Y.; Meng, Y.; Zare, R. N. Positively Charged Water Microdroplets Ionize Surrounding Gas Molecules. *J. Am. Soc. Mass. Spectrom.* **2025**, *36* (9), 1856−1859.
(51) Xie, R.; Guo, K.; Li, Y.; Zhang, Y.; Zhong, H.; Leung, D. Y. C.; Huang, H. Harnessing air-water interface to generate interfacial ROS for ultrafast environmental remediation. *Nat. Commun.* **2024**, *15* (1), 8860.
(52) Mofidfar, M.; Mehrgardi, M. A.; Xia, Y.; Zare, R. N. Dependence on relative humidity in the formation of reactive oxygen species in water droplets. *Proc. Natl. Acad. Sci. U. S. A.* **2024**, *121* (12), No. e2315940121.
(53) Xing, D.; Meng, Y.; Yuan, X.; Jin, S.; Song, X.; Zare, R. N.; Zhang, X. Capture of Hydroxyl Radicals by Hydronium Cations in Water Microdroplets. *Angew. Chem., Int. Ed.* **2022**, *61* (33), No. e202207587.
(54) Qiu, L.; Cooks, R. G. Simultaneous and Spontaneous Oxidation and Reduction in Microdroplets by the Water Radical Cation/Anion Pair. *Angew. Chem., Int. Ed.* **2022**, *61* (41), No. e202210765.
(55) Jia, X.; Wu, J.; Wang, F. Water-Microdroplet-Driven Interface-Charged Chemistries. *JACS Au* **2024**, *4* (11), 4141−4147.
(56) Enami, S. Can Hydroxyl Radicals Be Spontaneously Formed at the Air-Water Interface of Microdroplets? A Spray Ionization Mass Spectrometry Study. *J. Phys. Chem. Lett.* **2025**, *16* (45), 11604−11609.
(57) Meng, Y.; Gnanamani, E.; Zare, R. N. Direct C(sp^3)-N Bond Formation between Toluene and Amine in Water Microdroplets. *J. Am. Chem. Soc.* **2022**, *144* (43), 19709−19713.
(58) Li, K.; Zhang, B.; Xia, D.; Ye, Z.; Pan, Y.; Francisco, J. S.; Mi, Z. Room-Temperature Catalyst-Free Ammonia Decomposition for Hydrogen Production on Water Microdroplets. *J. Am. Chem. Soc.* **2025**, *147* (24), 20417−20425.

(59) Nandy, A.; Banerjee, S. Aqueous Microdroplets Induce the Metamorphosis of Indole into Quinazolinone Pharmacophores. *J. Am. Chem. Soc.* **2025**, *147* (45), 41242−41247.
(60) Bose, S.; Mofidfar, M.; Zare, R. N. Direct Conversion of N2 and Air to Nitric Acid in Gas-Water Microbubbles. *J. Am. Chem. Soc.* **2024**, *146* (40), 27964−27971.
(61) Mehrgardi, M. A.; Mofidfar, M.; Li, J.; Chamberlayne, C. F.; Lynch, S. R.; Zare, R. N. Catalyst-Free Transformation of Carbon Dioxide to Small Organic Compounds in Water Microdroplets Nebulized by Different Gases. *Advanced Sci.* **2024**, *11* (38), 2406785.
(62) Chen, X.; Xia, Y.; Zhang, Z.; Hua, L.; Jia, X.; Wang, F.; Zare, R. N. Hydrocarbon Degradation by Contact with Anoxic Water Microdroplets. *J. Am. Chem. Soc.* **2023**, *145* (39), 21538−21545.
(63) Tampieri, F.; Ginebra, M.-P.; Canal, C. Quantification of Plasma-Produced Hydroxyl Radicals in Solution and their Dependence on the pH. *Anal. Chem.* **2021**, *93* (8), 3666−3670.
(64) Liu, J.; Zheng, Z.; Wang, N.; Li, G. Plasma-Droplet Fusion-Mass Spectrometry Reveals Sub-Millisecond Protein Unfolding Dynamics Induced by Reactive Oxygen Species. *Anal. Chem.* **2024**, *96* (6), 2292−2296.
(65) Privat-Maldonado, A.; Schmidt, A.; Lin, A.; Weltmann, K.-D.; Wende, K.; Bogaerts, A.; Bekeschus, S. ROS from Physical Plasmas: Redox Chemistry for Biomedical Therapy. *Oxidative Medicine and Cellular Longevity* **2019**, *2019* (1), 9062098.
(66) Ji, W.-O.; Lee, M.-H.; Kim, G.-H.; Kim, E.-H. Quantitation of the ROS production in plasma and radiation treatments of biotargets. *Sci. Rep.* **2019**, *9* (1), 19837.
(67) Zhou, H.; Yang, R.; Jin, X.; Zhou, M. Infrared Spectra of the OH^+ and H_2O^+ Cations Solvated in Solid Argon. *J. Phys. Chem. A* **2005**, *109* (27), 6003−6007.
(68) Gruebele, M. H. W.; Müller, R. P.; Saykally, R. J. Measurement of the rotational spectra of OH+ and OD+ by laser magnetic resonance. *J. Chem. Phys.* **1986**, *84* (5), 2489−2496.

https://doi.org/10.1021/acs.jpclett.5c03405
J. Phys. Chem. Lett. 2026, 17, 389−396